POLITECNICO DI TORINO
Repository ISTITUZIONALE

Ionizing radiation profiling through the induced refractive index change in backscattering-enhanced optical fibers

(Article begins on next page)

08 November 2022

PROCEEDINGS OF SPIE

Ionizing radiation profiling through the induced refractive index change in backscattering-enhanced optical fibers

Massimo Olivero, Aurora Bellone, Martha Segura Sarminento, Wilfried Blanc, Franck Mady, et al.

SPIE.

Ionizing radiation profiling through the induced refractive index change in backscattering-enhanced optical fibers

Massimo Olivero[a], Aurora Bellone[a], Martha Segura[a], Wilfried Blanc[b], Franck Mady[b], Mourad Benabdesselam[b], Daniele Tosi[c], and Guido Perrone[a]

[a]Politecnico di Torino, DET, Corso Duca degli Abruzzi, 24 - 10129, Torino, Italy
[b]Université Côte d'Azur, CNRS, Institut de Physique de Nice, Grand Château,28 Avenue de Valrose - 06103, Nice, CEDEX
[c]Nazarbayev University, 53 Kabanbay Batyr Ave, Nur-Sultan city, Republic of Kazakhstan, 010000

ABSTRACT

Enhanced Rayleigh backscattering optical fibers, interrogated by an optical frequency domain reflectometer, are used to perform remote real-time measurements of X-ray irradiation profiles, with possible application as dosimeters in radiotherapy treatments. The enhanced Rayleigh backscattering is obtained by proper engineering of the composition of fiber core, either by introduction of Aluminum or Magnesium silicate nanoparticles as radiation-sensitive dopants. A detectable radiation-induced refractive index change can be spatially resolved through the measurement of the frequency shift of the Rayleigh backscattering along the fiber. It is experimentally demonstrated that two mechanisms of radiation-induced refractive index change take place. At doses nearly compatible with those delivered in radiotherapy, a negative refractive index is induced, whereas at high doses the change is positive. This behavior is also confirmed by the shift of Bragg wavelength of a fiber Bragg grating inscribed in the nanoparticles-doped fiber and used as a reference.

Keywords: Optical fiber sensors, Radiation monitoring, Radiation dosage, Ionizing radiation sensors

1. INTRODUCTION

Medical applications of ionizing radiations are the subject of a number of research lines that range from diagnosis to therapy and often require a precise measurement of the radiation dose. Furthermore, medical protocols related to exposure to ionizing radiation involve an accurate dose monitoring for the safety of the patient as well as the medical staff. Besides the applied dose rate and the total dose delivered, a key parameter is the radiation distribution in the target volume. Hand-held detectors cannot perform such a measurement in-situ and in real time. GafChromic (GaF) films[1] or gel-based nano-sensors[2] allow to measure the dose and its spatial distribution. However, these two sensors are not suitable for continuous and real-time dose measurements[3] and they may be tricky to be positioned in the target area.

A possible and interesting solution for in-situ, real-time dose profiling is represented by optical fibers used as radiation sensors, thanks to their features: minimal invasiveness, remote interrogation, electromagnetic insensitivity and passive operation (i.e. absence of electrical currents). The exposure of an optical fiber to ionizing radiations causes the Radiation Induced Attenuation (RIA) that is, a local increment of the propagation loss in the exposed length. With this effect, it is possible to measure the loss distribution along the length of the fiber which is then related to the profile of the radiation intensity. Another possible physical modification due to radiation is a radiation-induced refractive index change (RIRIC) of the core-cladding structure. Standard telecom optical fibers are devised to undergo harsh environments and usually designed to have low sensitivity to ionizing radiation. Special radiation-resistant fibers are also commercialized, which can tollerate doses up to MGy with acceptable RIA. RIRIC is normally not taken into account because it does not impair the communication and its behavior is not reported in datasheets. Therefore, optical fiber dosimetry requires the development of specially

---

Further author information: (Send correspondence to Massimo Olivero)
Massimo Olivero: E-mail: massimo.olivero@polito.it, Telephone: +39 0112276311

designed fibers, namely enhanced backscattering fibers (EBFs), that exhibit enough sensitivity to radiation in the form of RIA or RIRIC (other effects such as radiation-induced luminescence or thermoluminescence[4] are not considered in this work).

In optical communications, the measurement propagation loss along an optical fiber, stemming from a number of causes (Rayleigh scattering, intrinsic defects in the glass matrix, physical damages, spectral loss due to absorption of some dopant or impurity etc.), can be performed by optical time domain reflectometry (OTDR). OTDR exploits the principle of radar, with that it measures the backscattering signal from a laser pulse travelling along the fiber. The backscattered signal, according to its power level and received time, yields the information about the localized propagation loss or the strength of any lumped defect along the fiber, as well as its position. OTDRs have been employed for the detection of long-range gamma-rays[5] and to evaluate the RIA of different optical fibers in physics experiments.[6] OTDR technique is not suitable for radiation dosimetry in biomedical applications because of a number of limitations e.g. the so-called dead zone (the reflectometer cannot detect any signals in the first meters of the fiber), the insufficient meter-size spatial resolution and the inadequate sensitivity for the detection of low levels of RIA.

Optical Frequency Domain Reflectometry (OFDR),[7] based on the optical schematic of Fig. 1, can overcome some of these limits and, besides RIA, it also give information about RIRIC.
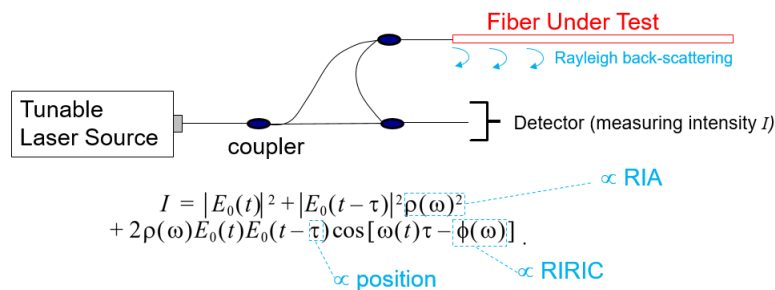

Figure 1. Schematic representation of the OFDR principle of operation. The intensity I measured by the detector contains information about the Radiation-Induced Refractive Index Change (RIRIC) and the Radiation-Induced Attenuation (RIA) along the fiber under test. $|E_0(t)|^2$ is the intensity provided by the tunable laser and $\rho(\omega)$ the spectral response of the device (in this case a fiber) under test; ω is related to the current wavelength of the swept laser and t and τ are the time and time delay of the observation. By performing autocorrelation and subsequent Fourier transform of I it is possible to evaluate RIA and RIRIC along the fiber.

The basic structure of an OFDR instrument consists of a swept wavelength laser, a modified Mach-Zender interferometer and two photodetectors. One arm of the interferometer has fixed length and works as reference, whereas the other is connected to the fiber under test. The interference obtained from the combination of backscattered light from the fiber under test and the reference arm signal brings information about the reflective events in term of magnitude and position, with a spatial resolution of fraction of millimeters. Unlike conventional interferometry, where the spatial information is retrieved by changing the length of the reference arm, here the changing parameter is the wavelength of the source. Multiple wavelength sweeps are performed in order to improve the quality of the backscattering signal. From a Fourier transform of the acquired data, it is possible to obtain an OTDR-like trace with sub-mm resolution and no dead zone. OFDR can also be used to characterise waveguide and fiber components such as fiber Bragg gratings (FBG) and monitor their evolution when they are used as sensors.

The present work reports on the investigations of X-ray exposure of two types of EBF, relying on Aluminium doping and Magnesium nanoparticles doping, respectively. The propagation loss profile of these fibers is acquired through OFDR and processed in order to find a correlation between RIRIC and radiation dose. The change of refractive index due to radiation is also investigated by exposing an FBG that has been previously recorded in the Magnesium nanoparticles doped fiber by femtosecond laser writing. The FBG changes its Bragg wavelength under X-ray exposure and can be used as a reference for RIRIC calculation. The present paper, extending the work published by the same authors,[8] compares in details the behaviour of the two fiber types, highlighting two different mechanisms on the RIRIC that take place at low and high dose.

2. SETUP AND METHODS

The enhanced backscattering fibers (EBFs) are fabricated as described by Cognolato[9] and by Blanc[10] in a two steps procedure, consisting in the fabrication of a preform by Modified Chemical Vapour Deposition (MCVD) followed by fiber drawing in a drawing tower. A solution-doping technique is applied to incorporate the dopants (Aluminium or Magnesium) in the core that has been previously deposited at a reduced temperature to make an unsintered porous soot. The formation of nanoparticles in the Magnesium doped fiber is caused by phase separation at high temperature, as described by Blanc.[11] The inscription of fiber Bragg gratings (FBGs), as reference sensors for RIRIC evaluation, is performed by femtosecond laser direct writing. The periodic structure is recorded through Point-by-Point (PbP) technique, by focusing pulses from a 515 nm laser (Carbide - Light Conversion) into the fiber core using a 0.75 NA, 100x long working distance objective. The fiber is immersed in index matching oil to reduce the aberration. The inscription pulse energy is around 200 nJ for a pulse duration of 243 fs and 1 kHz repetition rate. The fiber is translated under the laser beam at proper speed and a shutter controls the laser exposure to produce the proper periodicity to record FBGs at wavelengths around 1550 nm.

The setup for characterisation of the EBFs, sketched in Fig. 2, includes the sensing fiber, the radiation chamber for X-ray exposure and the optical frequency domain reflectometer (OBR4600 by Luna Technologies®[12]). The reflectometer produces an OTDR-like trace (backscattering power vs fiber position) with a spatial resolution that can be as low as 10 μm, depending on the wavelength sweep performed by the tunable laser source, which emits in the range 1520 nm–1630 nm. Not shown in Fig. 2, the setup also includes an FBG interrogator to track the Bragg wavelength of the FBGs under exposure. The EBF under test is connected to either interrogator by a standard single mode (SMF) pigtail with angled connector, to keep as low as possible spurious reflections. The connection between EBF and SMF is performed with fusion splicing using a standard recipe for single mode fiber splicing.
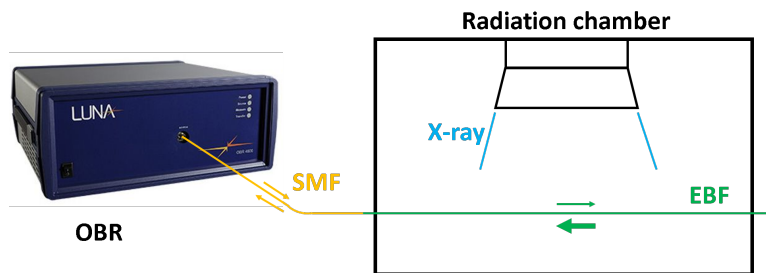

Figure 2. Schematic representation of the measurement setup.

The acquisitions from the OFDR are automatically performed thanks to an on purpose-made Labview™ program that pushes the acquisition rate to the limit set by the parameters of the OFDR, which is set in "sensing mode". In this configuration mode, a reference backscattering trace is acquired prior to exposure; the acquisitions during X-ray radiation are then cross-correlated to the reference in order to calculate the spectral shift (expressed in GHz or pm) that the backscattering signal has experienced due to local changes of refractive index along the fiber. In sensing mode, three parameters influence the acquisition rate and the achievable spatial resolution, namely the sensing range, the gage length and the sensor spacing. The fiber under test can be thought as a cascade of Bragg gratings having a length equal to the gage length and separated by sensor spacing, whereas the total length of the equivalent FBG array is represented by the sensing range. In the experiments hereby reported the sensor spacing was set at the minimum of 0.16 mm, the gage length at 30 mm and the sensing range at 1 m, resulting in a delay of 10 s between two consequent acquisitions. Faster acquisitions could be performed by reducing the gage length, at a price of reduced sensitivity and increased delay between acquisitions. The fiber under exposure is fastened on a support under the X-ray beam, so that the spectral shift can only be ascribed to the effect of radiation, without any spurious effect of strain. Temperature variations are also considered negligible in the constant-temperature lab environment. The delivered dose rate is controlled by changing both the electric current supplied to the X-ray emitter and by changing the distance between the emitter and the fiber. The distance from the emitter controls the illumination cone (sketched in Fig. 2), hence the length of the fiber irradiated with X-rays. The fibers under test were exposed to high (about 700 Gy/min) and low (2 Gy/min) dose

rates. The latter may be compatible with dose rates used in Flash-RT[13] and thus represent a working condition for real applications.

3. RESULTS AND DISCUSSION

The results hereby reported refer to two EBFs labeled M01 and R08. M01 is doped with Magnesium nanoparticles, while R08 is doped with Aluminum. Fig. 3 depicts the Rayleigh backscattering curve of M01. The curve exhibits two reflection peaks that correspond to the splicing with SMF28 pigtails. These may be due to slight mismatch of both refractive index and dimension between M01 and SMF28. It can be observed that the level of scattering is enhanced by about 30 dB (from about −100 dB to about −70 dB) with respect to the SMF28 pigtails in which the fiber is sandwiched. Further, it can be noticed the high attenuation of the fiber, given the high slope of the curve (about 10 dB) over a length of 30 cm between the two positions 3.7 m and 4 m.
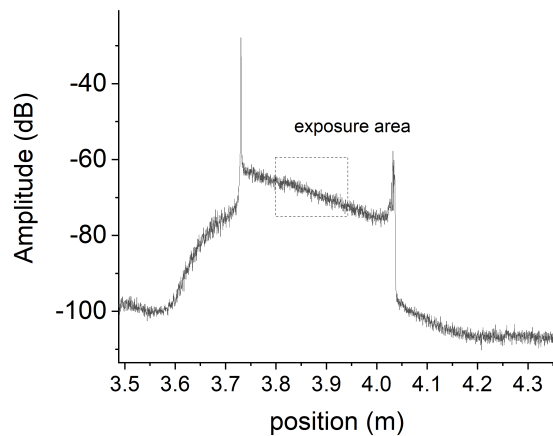

Figure 3. Rayleigh backscattering of fiber M01 containing Magnesium nanoparticles. The two peaks correspond to the splicing to standard SMF28 pigtails.

As a comparison, the fiber R08 with Aluminium doped core exhibits a much lower backscattering (around −120 dB) and negligible loss on a cm scale, as well as no reflective or loss effects at the splice with SMF28 pigtails. These features are observable in Fig. 4.
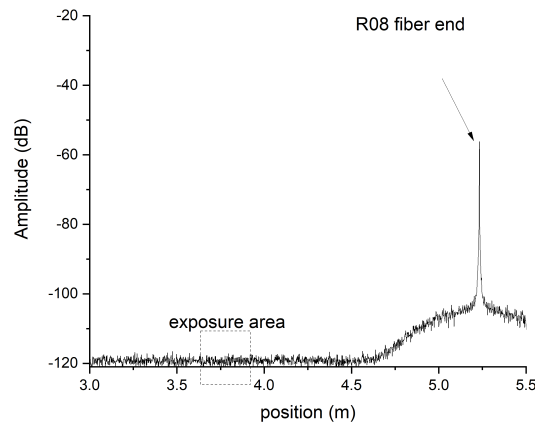

Figure 4. Rayleigh backscattering of fiber R08 doped with Aluminium. This fiber exhibits low propagation loss and perfect matching to SMF28 pigtail, since there is not reflection or attenuation at the splice located at position around 3.5 m.

The recorded spectral shifts at high dose rate as a function of position, reported in Fig. 5 and Fig. 6, demonstrate that both are responsive to the exposure, with a higher spectral shift recorded for the Aluminium-doped fiber R08.
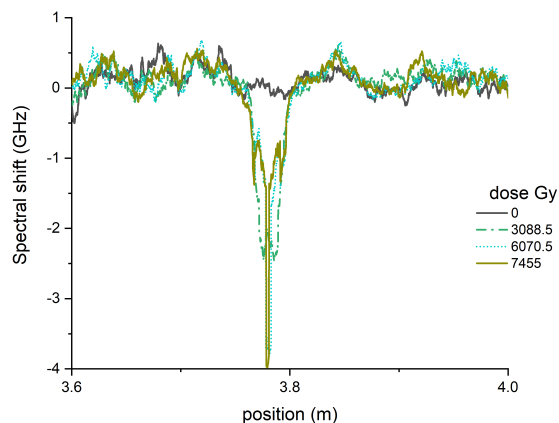

Figure 5. Fiber R08 (Aluminium-doped): spectral shift vs position for exposure at 700 Gy/min. Exposure has been performed at position about 3.8 m.
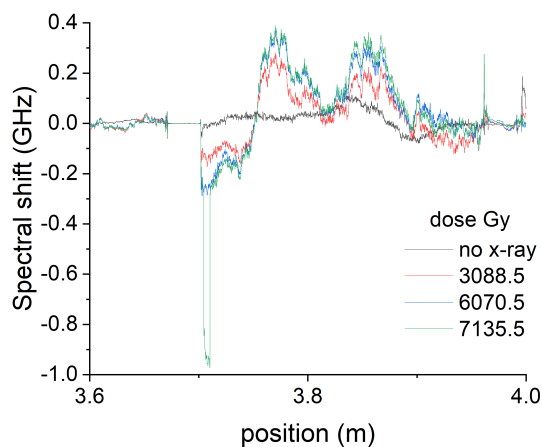

Figure 6. Fiber M01 (Magnesium nanoparticles): spectral shift vs position for exposure at 700 Gy/min. Exposure has occurred at position 3.7 m.

The evolution of the spectral shift is then reported in Fig. 7 and Fig. 8, where it is plotted as a function of total delivered dose, showing a trend toward negative values with a higher and nearly linear slope for fiber R08 and a more abrupt change around 7000 Gy for fiber M01.
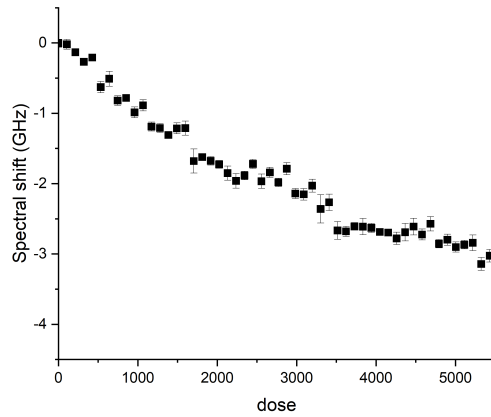
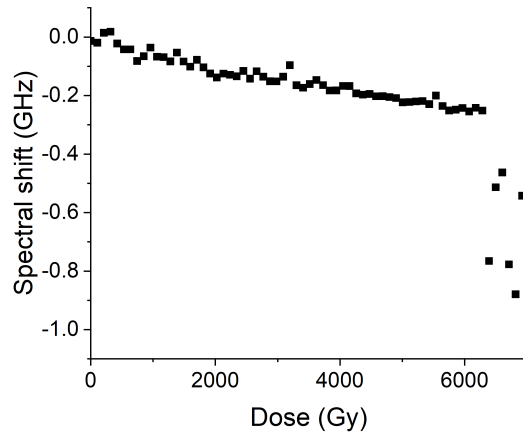Figure 7. Fiber R08 (Aluminium-doped): spectral shift vs dose, for exposure at $700\,\mathrm{Gy/min}$.

Figure 8. Fiber M01 (Magnesium nanoparticles): spectral shift vs dose, for exposure at $700\,\mathrm{Gy/min}$.

A negative spectral shift corresponds to an equivalent positive change of the induced refractive index, i.e. $\Delta f/f = -\Delta\lambda/\lambda = -\Delta n/n$. Since the interrogation wavelengths of the OFDR are around $1570\,\mathrm{nm}$ (corresponding to $190.951\,\mathrm{THz}$), it turns out that the RIRIC is in the order of 6e-6 for the fiber M01. On the same fiber, a Bragg grating was inscribed at $1537\,\mathrm{nm}$ with femtosecond laser, using the procedure previously described, and a radiation-induced Bragg shift of $14\,\mathrm{pm}$ was recorded (cfr Fig. 9). The latter corresponds to a change of effective refractive index of about 9e-6, which is in reasonable agreement with the OFDR measurement. The physical mechanisms behind the measured spectral shift in the pristine M01 fiber and the Bragg shift of the photo-written FBG under X-ray exposure may also be different, but the rationale of this experiment is mainly to confirm that the fiber has some sensitivity to radiation and to confirm the possibility to perform distributed sensing with the OFDR or quasi-distributed sensing with standard FBGs.
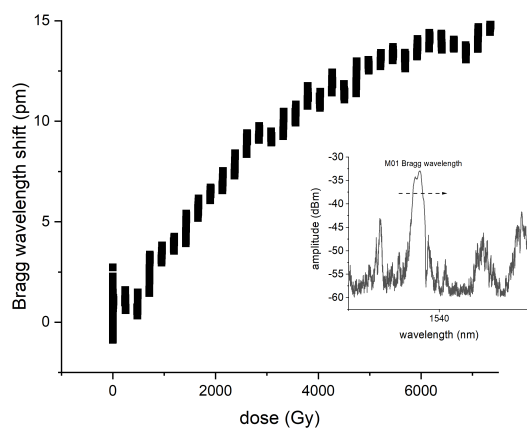
Figure 9. Bragg wavelength shift of a FBG inscribed in Fiber M01 (Magnesium nanoparticles) and exposed at 700 Gy/min. The inset depicts the spectrum of the FBG prior to exposure with an arrow indicating the versus of the shift.

Exposures at low dose rate of 2 Gy/min yield an opposite change of refractive index, as it can be observed in Fig. 10 and 11. A spectral shift up to 1 GHz is observed for the Aluminium-doped fiber R08 when the total dose reaches about 7000 Gy. The Magnesium nanoparticles doped fiber M01 exhibits a shallow spectral shift, close to the measurement noise.
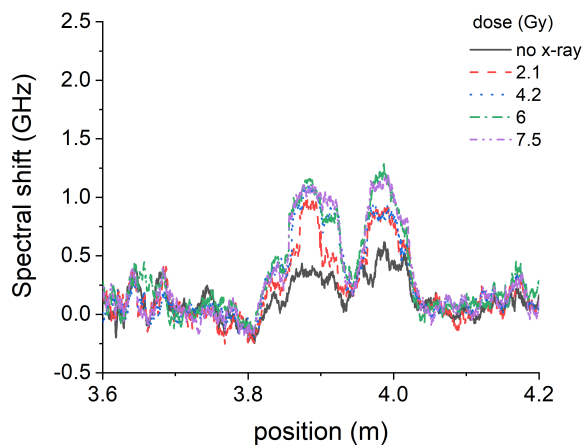

Figure 10. Fiber R08 (Aluminium-doped): spectral shift vs position for exposure at 2 Gy/min. Notice a positive evolution of the spectral shift.
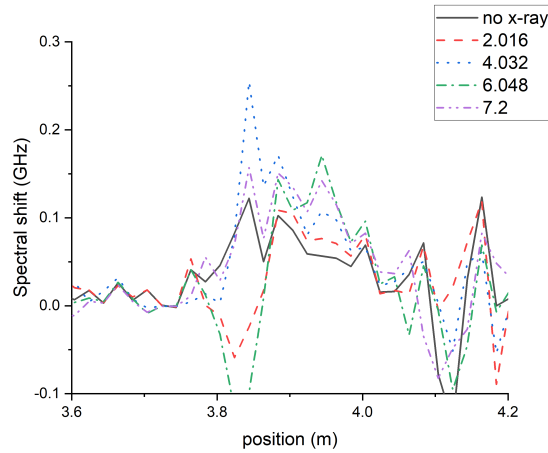
Figure 11. Fiber M01 (Magnesium nanoparticles): spectral shift vs position for exposure at $2\,\mathrm{Gy/min}$.

This becomes clear from Fig. 13 reporting the spectral shift as a function of the total dose delivered, where a small increment of the spectral shift can be inferred by averaging the data before and after exposure, though a clear trend is not displayed, since the measures exhibit a large variation due to the noise fluctuations during the acquistion. Aluminium-doped fiber R08 exhibits a higher sensitivity, as reported in Fig. 12, as well as a clear dependence upon the total dose. However, also this measurement is affected by large fluctuations, as proved by the large error bars.
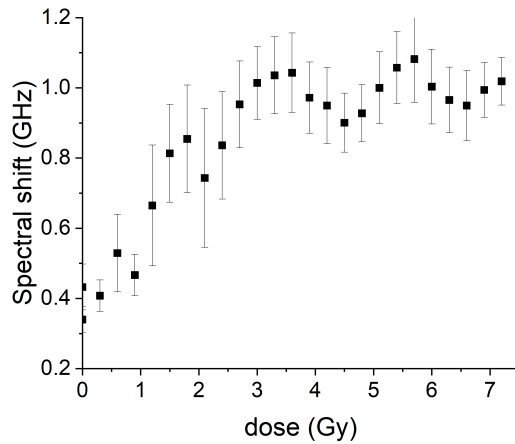

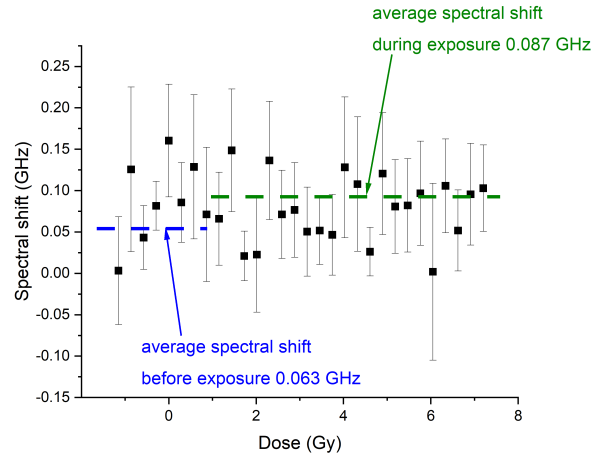Figure 12. Fiber R08 (Aluminium-doped): spectral shift vs dose at dose rate of $2\,\mathrm{Gy/min}$.

Figure 13. Fiber M01 (Magnesium nanoparticles): spectral shift vs at dose rate of $2\,\text{Gy/min}$.

An interesting feature observable in Fig. 10 is the dip at the center of the spectral shift profile where the intensity of the X-ray beam is supposed to be higher. This is very likely due to the competing mechanism of refractive index change that produces a negative spectral shift as observed for high doses. Another interesting feature of the spectral shift profiles at low dose of Fig. 10 and 11 is that they indicate an X-ray beam profile of width about $20\,\text{cm}$, which is a 5-fold larger than that measured at high dose in Fig. 5 and Fig. 6. This is qualitatively in agreement with the diverging X-ray beam depicted in Fig. 2, despite the the beam sizes recorded with a GaF sheet yielded lower diameters. However, The GaF measure was also qualitative, since a colorimetric scale was not available. Quantitative measurements shall be carried out by an X-ray beam profiler (e.g. those based on scanning slit) so that a a more reliable spatial calibration of the sensing fiber should be possible. In summary, both fibers are responsive to X-rays at high and low doses, exhibiting a RIRIC that is detectable by OFDR as spectral shift of the Rayleigh backscattering. The mechanism of RIRIC is different at high and low dose; in particular a lowering of the local refractive index occurs for low level doses. The Aluminium-doped fiber exhibits higher sensitivity and appears a better candidate for radiation-dose profiling. On the other hand, the Magnesium nanoparticles doped fiber could be exploited for its lower sensitivity to X-rays in the opposite way, e.g. it could be better used in radiation environments as a radiation-insensitive distributed temperature sensor, as it has already been devised by Beisenova et al.[14]

4. CONCLUSION

The presented work has investigated the use of enhanced backscattering optical fibers in conjunction with optical frequency domain reflectometry for real-time, in-situ dose profiling of X-ray radiation. Two custom designed optical fibers, with the core doped with Aluminium and Magnesium nanoparticles respectively, have been tested in a radiation chamber and exposed to X-rays at dose rates ranging from high value of $700\,\text{Gy/min}$ down to nearly therapeutic levels of $2\,\text{Gy/min}$. The spectral shift of the backscattering signature has been recorded in real time during the X-ray exposure, highlighting two different mechanisms of refractive index change along the exposed section of the sensing fiber. In details, a high dose rate produces a negative spectral shift corresponding to an increment of refractive index, whereas a low dose rate produces the opposite effect. This behaviour holds for both fiber types, with the Aluminium doped fiber being more responsive. The refractive index change has also been verified by a Bragg grating recorded into the Magnesium nanoparticles-doped fiber that exhibits a shift of the Bragg wavelength indicating a radiation-induced change of the refractive index comparable with that measured by optical frequency domain reflectometry. The overall investigation shows a potential for the ensemble enhanced backscattering fiber + optical time domain reflectometry, though the results demand for further analyses and new experiments. Further improvements shall include: 1) testing new dopants for enhanced sensitivity, 2) quantitative calibration of the X-ray beam distribution and 3) an extensive testing at different dose

rates and delivered doses, with focus on the values that are used both in conventional and advanced radiotherapy treatments.

REFERENCES

[1] A. Micke, D. F. Lewis, and X. Yu, "Multichannel film dosimetry with nonuniformity correction," in *Med. Phys*, 2523–2534, vol. 38 (2011).

[2] K. Pushpavanam, S. Inamdar, S. Dutta, *et al.*, "Determination of topographical radiation dose profiles using gel nanosensors," *Science Advances* **5** (2019).

[3] A. L. Palmer, P. Di Pietro, S. Alobaidli, *et al.*, "Comparison of methods for the measurement of radiation dose distributions in high dose rate (hdr) brachytherapy: Ge-doped optical fiber, ebt3 gafchromic film, and presage® radiochromic plastic," *Med Phys* **40**.

[4] M. Benabdesselam, J. Bahout, F. Mady, *et al.*, "TL Properties of RE-Doped and Co-Doped Sol-Gel Silica Rods. Application to Passive (OSL) and Real-Time (RL) Dosimetry," *IEEE Sensors Journal* **21**, 27465–27472 (2021).

[5] M. A. S. Zaghloul, A. Yan, R. Chen, *et al.*, "High spatial resolution radiation detection using distributed fiber sensing technique," *IEEE Transactions on Nuclear Science* **64**, 2569–2577 (2017).

[6] D. D. Francesca, G. L. Vecchi, S. Girard, *et al.*, "Qualification and calibration of single-mode phosphosilicate optical fiber for dosimetry at cern," *Journal of Lightwave Technology* **37**(18), 4643–4649 (2019).

[7] Z. Ding, C. Wang, K. Liu, *et al.*, "Distributed optical fiber sensors based on optical frequency domain reflectometry: A review," *Sensors* **18**, 1072 (2018).

[8] M. Olivero, A. Mirigaldi, V. Serafini, *et al.*, "Distributed x-ray dosimetry with optical fibers by optical frequency domain interferometry," *IEEE Transactions on Instrumentation and Measurement* **70**, 1–9 (2021).

[9] L. Cognolato, "Chemical vapour deposition for optical fibre technology," *Journal de Physique IV Proceedings* **5**, C5–975–987 (1995).

[10] W. Blanc, V. Mauroy, L. Nguyen, *et al.*, "Fabrication of rare earth-doped transparent glass ceramic optical fibers by modified chemical vapor deposition," *Journal of the American Ceramic Society* **94**, 2315–2318 (2011).

[11] W. Blanc, I. Martin, H. Francois-Saint-Cyr, *et al.*, "Compositional changes at the early stages of nanoparticles growth in glasses," *The Journal of Physical Chemistry C* **123**, 29008–29014 (2019).

[12] *LUNA OBR 4600 manual*.

[13] K. J. Harrington, "Ultrahigh Dose-rate Radiotherapy: Next Steps for FLASH-RT," *Clinical Cancer Research* **25**, 3–5 (2019).

[14] A. Beisenova, A. Issatayeva, S. Korganbayev, *et al.*, "Simultaneous Distributed Sensing on Multiple MgO-Doped High Scattering Fibers by Means of Scattering-Level Multiplexing," *Journal of Lightwave Technology* **37**, 3413–3421 (2019).